Supplementary Information

Doubly charged single Weyl pair with complete spin polarization

Shiwei Zhang[1,2,†], Ying Liu[3,†], Xiaoming Zhang[1,3], Peng Wang[1], Anlong Kuang[1], Zhenxiang Cheng[4], Hongkuan Yuan[1,*] and Tie Yang[1,2,*]

[1] School of Physical Science and Technology, Southwest University, Chongqing 400715, China

[2] College of Physics, Chongqing University, Chongqing 400044, China

[3] School of Materials Science and Engineering, Hebei University of Technology, Tianjin, 300130, China

[4] Institute for Superconducting and Electronic Materials, Faculty of Engineering and Information Sciences, University of Wollongong, Wollongong 2500, Australia

[†] These authors contribute equally to this work

[*] Emails: yhk10@swu.edu.cn and yangtie@swu.edu.cn

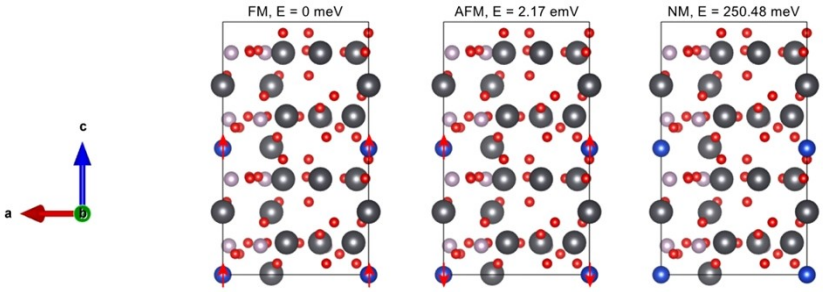

Figure S1. The relative energies for ferromagnetic (FM), antiferromagnetic (AFM), and nonmagnetic (NM) states in a 1 × 1 × 2 supercell of Cu doped lead apatite $Pb_9Cu(PO_4)_6O$. The arrows only indicate the spin directions of the Cu atoms.

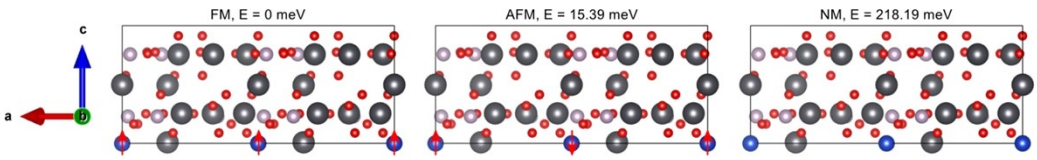

Figure S2. The relative energies for ferromagnetic (FM), antiferromagnetic (AFM), and nonmagnetic (NM) states in a 2 × 1 × 1 supercell of Cu doped lead apatite $Pb_9Cu(PO_4)_6O$. The arrows only indicate the spin directions of the Cu atoms.

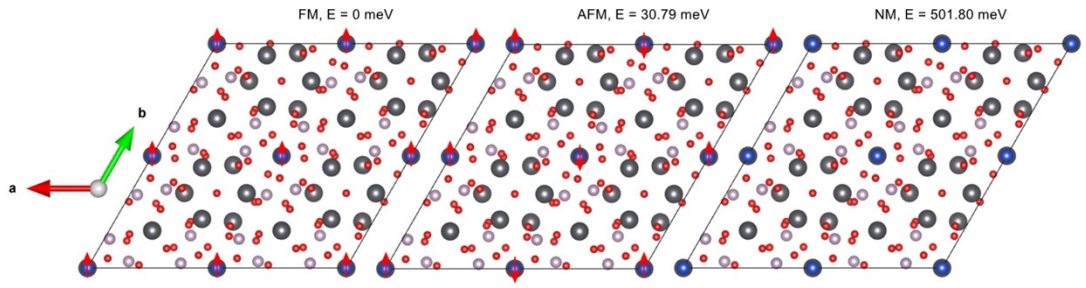

Figure S3. The relative energies for ferromagnetic (FM), antiferromagnetic (AFM), and nonmagnetic (NM) states in a 2 × 2 × 1 supercell of Cu doped lead apatite $Pb_9Cu(PO_4)_6O$. The arrows only indicate the spin directions of the Cu atoms.

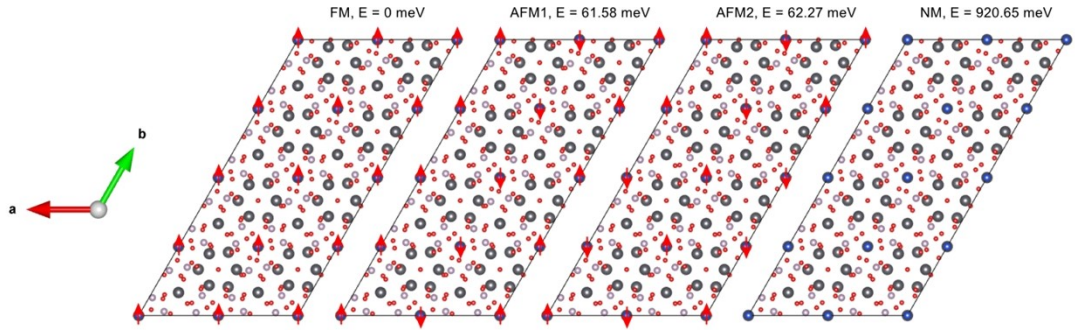

Figure S4. The relative energies for ferromagnetic (FM), antiferromagnetic 1 (AFM1), antiferromagnetic 2 (AFM2), and nonmagnetic (NM) states in a 2 × 4 × 1 supercell of Cu doped lead apatite $Pb_9Cu(PO_4)_6O$. The arrows only indicate the spin directions of the Cu atoms.

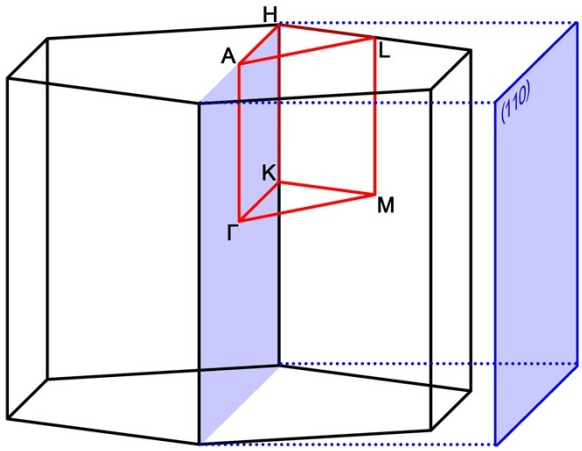

Figure S5. The Brillouin zone of Cu doped lead apatite $Pb_9Cu(PO_4)_6O$. The high symmetry paths are highlighted with red color lines and the corresponding high symmetry points are indicated by the corresponding labels. The color shaded area indicates the (110) surface projection.

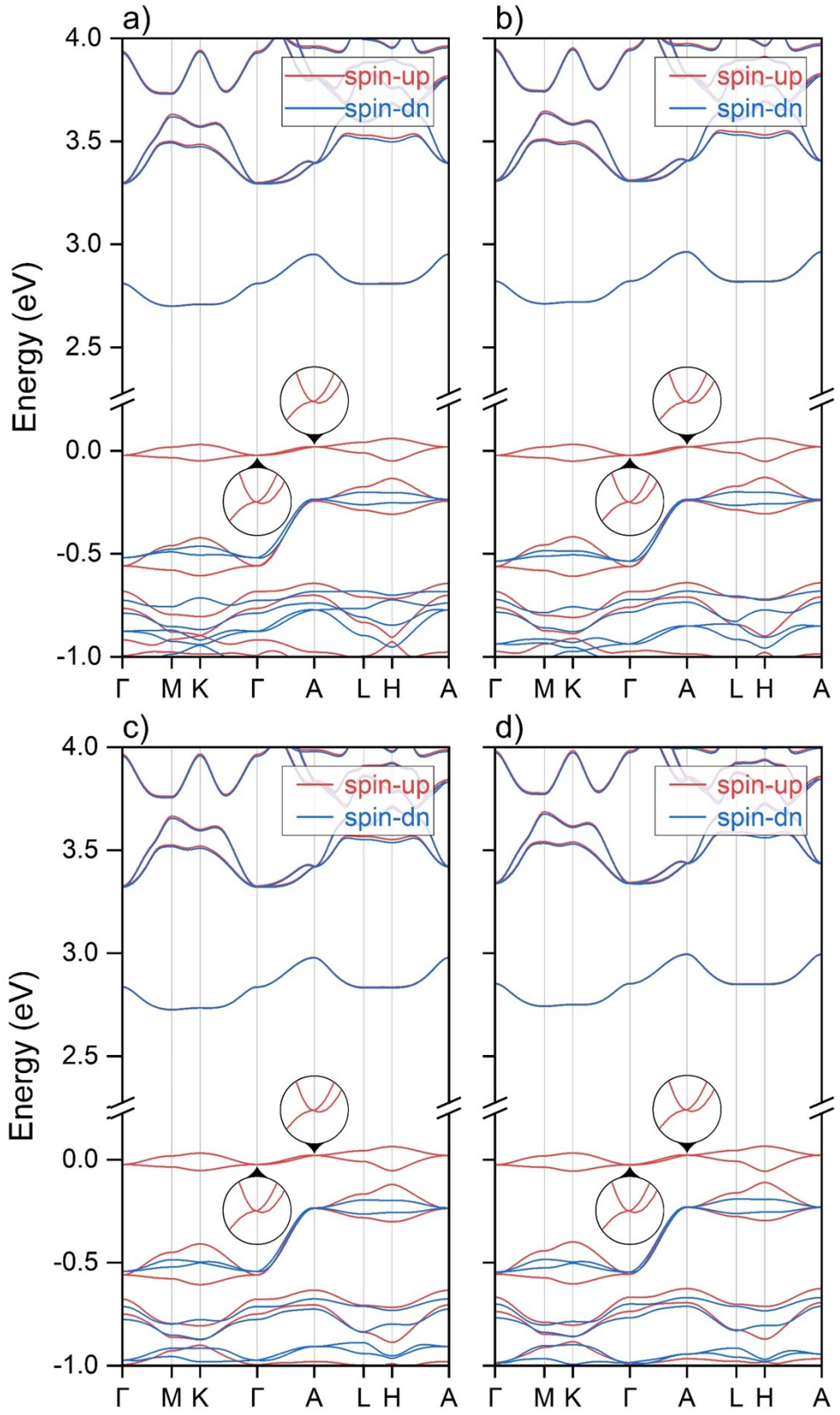

Figure S6. The spin polarized electronic band structures of the Cu doped lead apatite $Pb_9Cu(PO_4)_6O$ with GGA+U method. The applied Hubbard U values are 1 eV a), 2 eV b) 3 eV c) and 4 eV d), respectively. The band crossing points in the spin-down channel are locally enlarged, with the zoomed-in views located alongside. The crossing conditions are not affected by the different Hubbard U values at all and all the type-III dispersions are maintained.

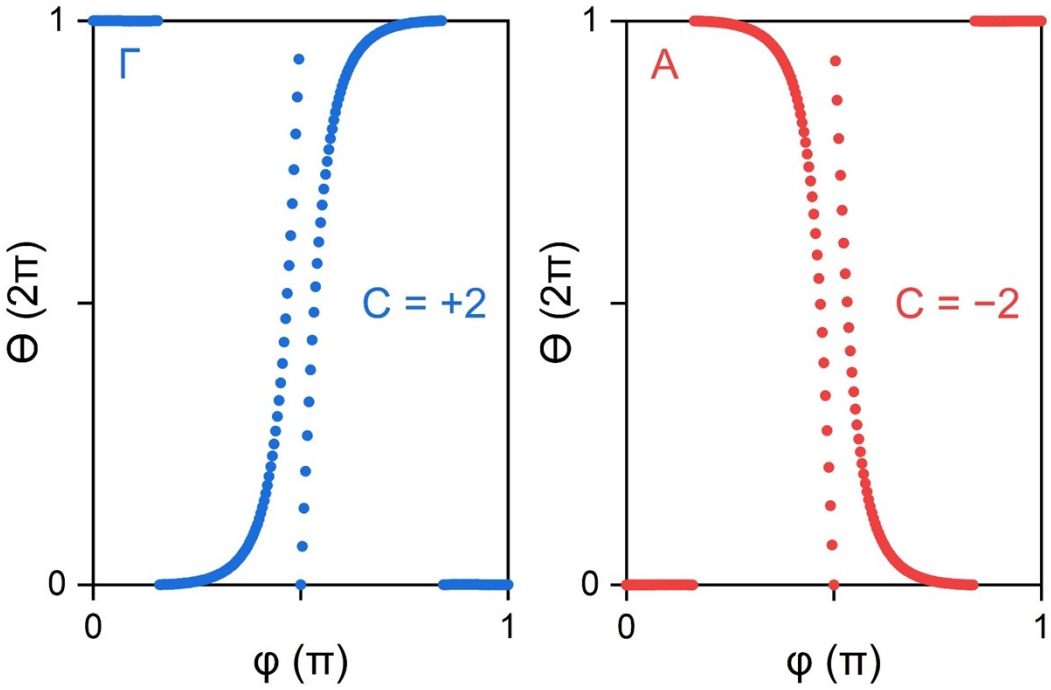

Figure S7. The evolutions of the average position of the Wannier center for the two Weyl points at Γ and A. The topological charge of +2 is derived for the Wely point at Γ, and the topological charge of -2 for the other Weyl point at A.

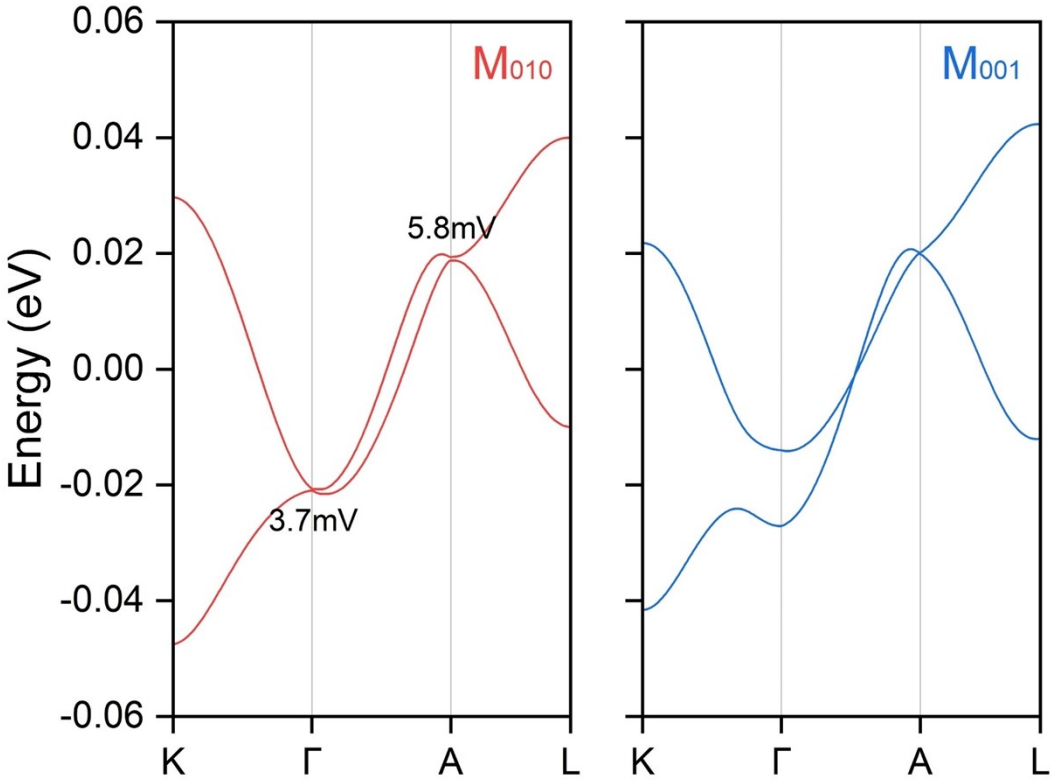

Figure S8. The electronic band structures of the Cu doped lead apatite $Pb_9Cu(PO_4)_6O$ with the consideration of the spin orbital coupling (SOC) effect. Two different magnetic directions are considered, as indicated by the color text, and the band crossings exhibit different conditions.

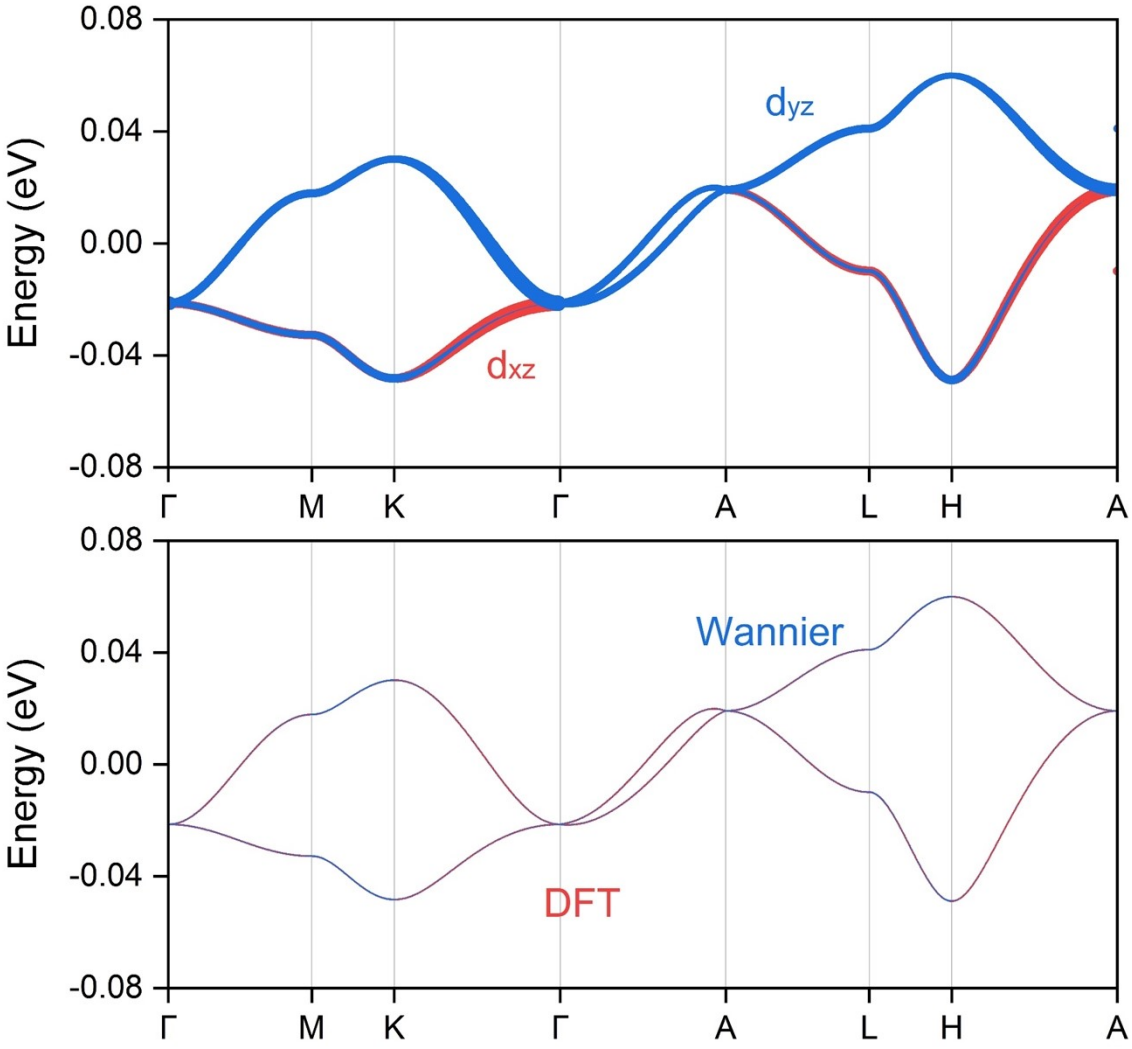

Figure S9. The electronic band structures of the Cu doped lead apatite $Pb_9Cu(PO_4)_6O$ with the orbital contribution projection from d_{xz} and d_{yz} of Cu in the top and Wannier fitting comparison with DFT calculation in the bottom.

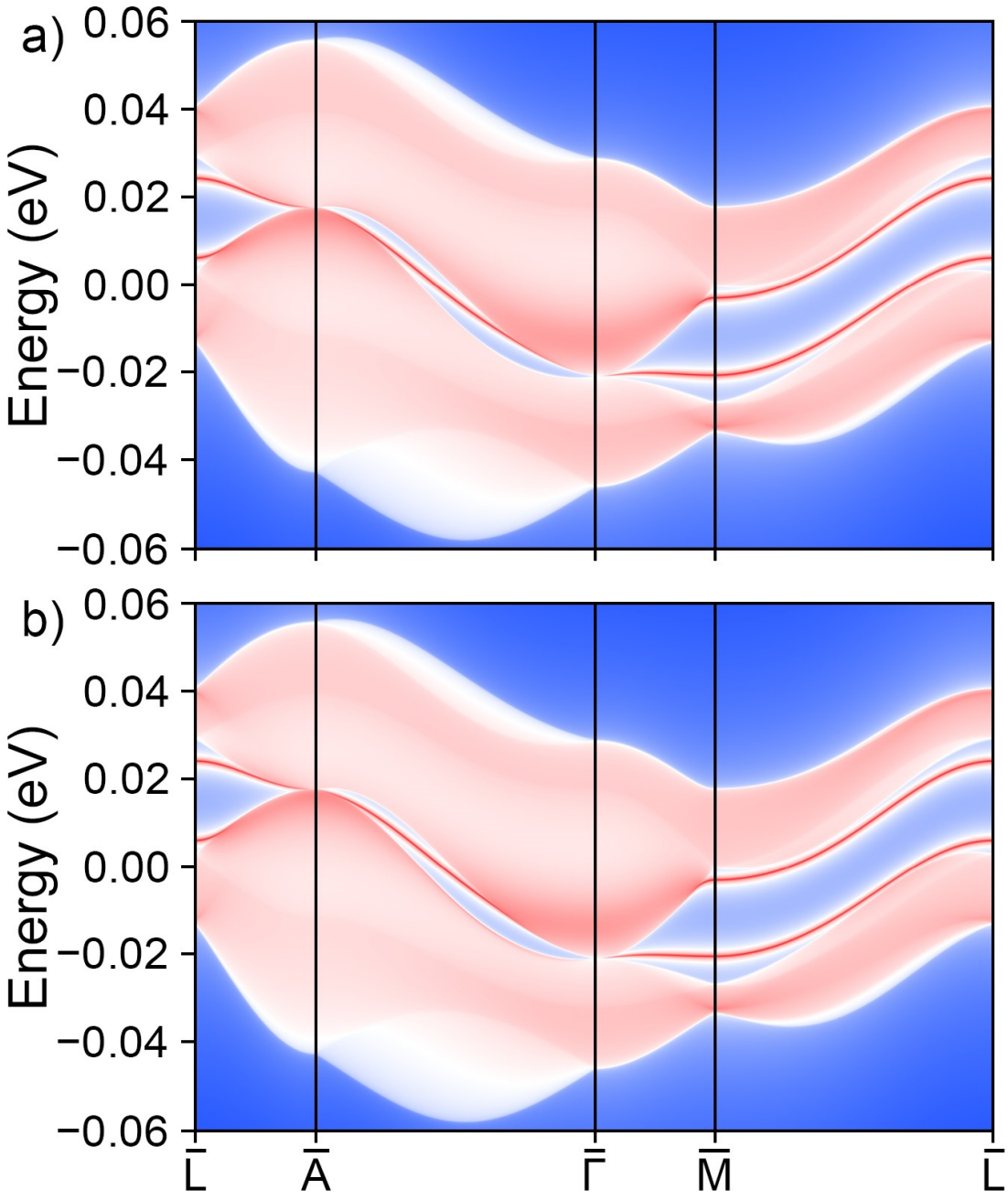

Figure S10. The projected surface states of $Pb_9Cu(PO_4)_6O$ in (100) plane for top a) and bottom b) terminations. Clear surface arc states connecting the Weyl points between at $\bar{\Gamma}$ and $\bar{A}$ positions can be easily distinguished from the bulk band states for both termination conditions.

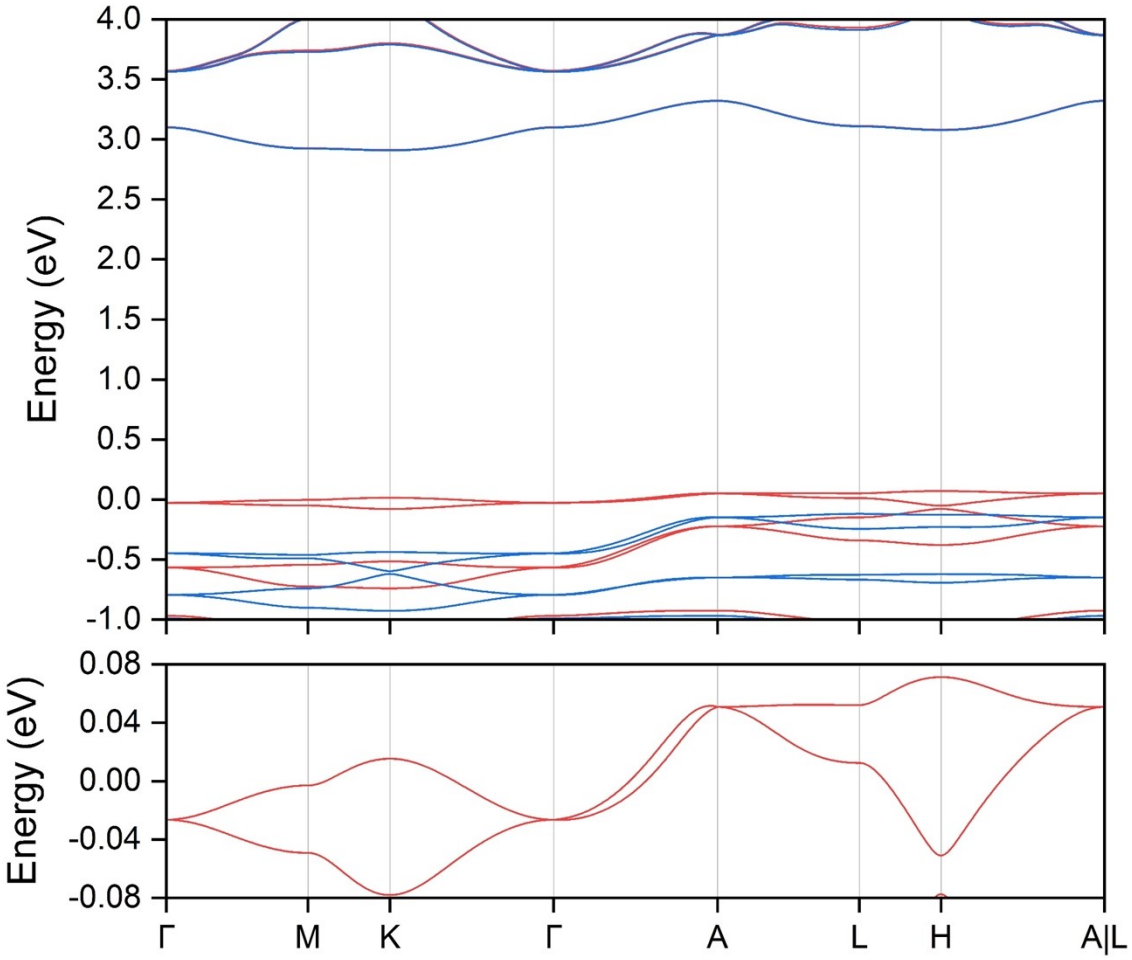

Figure S11. The spin polarized electronic band structures of the Cu doped lead apatite $Pb_9Cu(PO_4)_6O$ under -10% uniform strain. The two bands are further enlarged in the bottom panel and only two band crossing points are present at Γ and A positions.

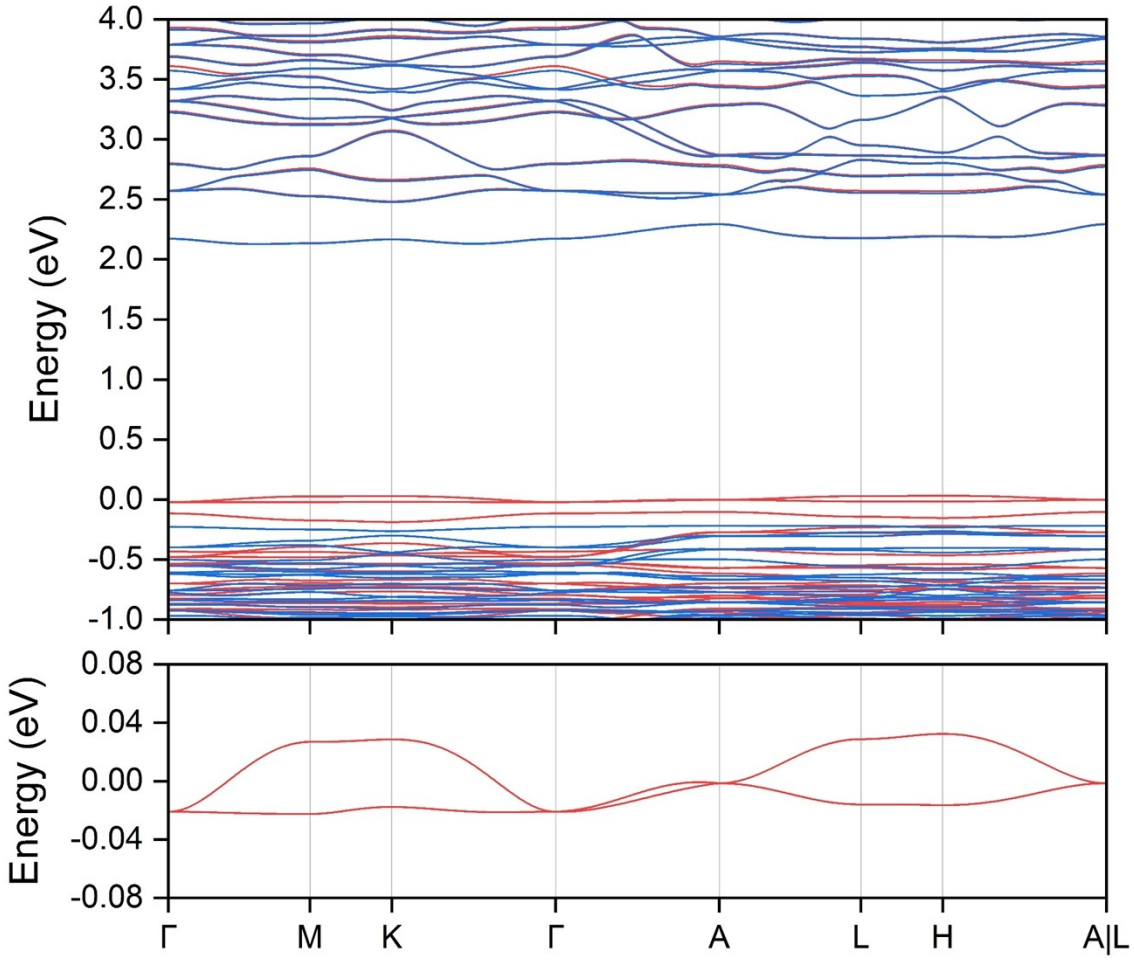

Figure S12. The spin polarized electronic band structures of the Cu doped lead apatite $Pb_9Cu(PO_4)_6O$ under +10% uniform strain. The two bands are further enlarged in the bottom panel and only two band crossing points are present at Γ and A positions.

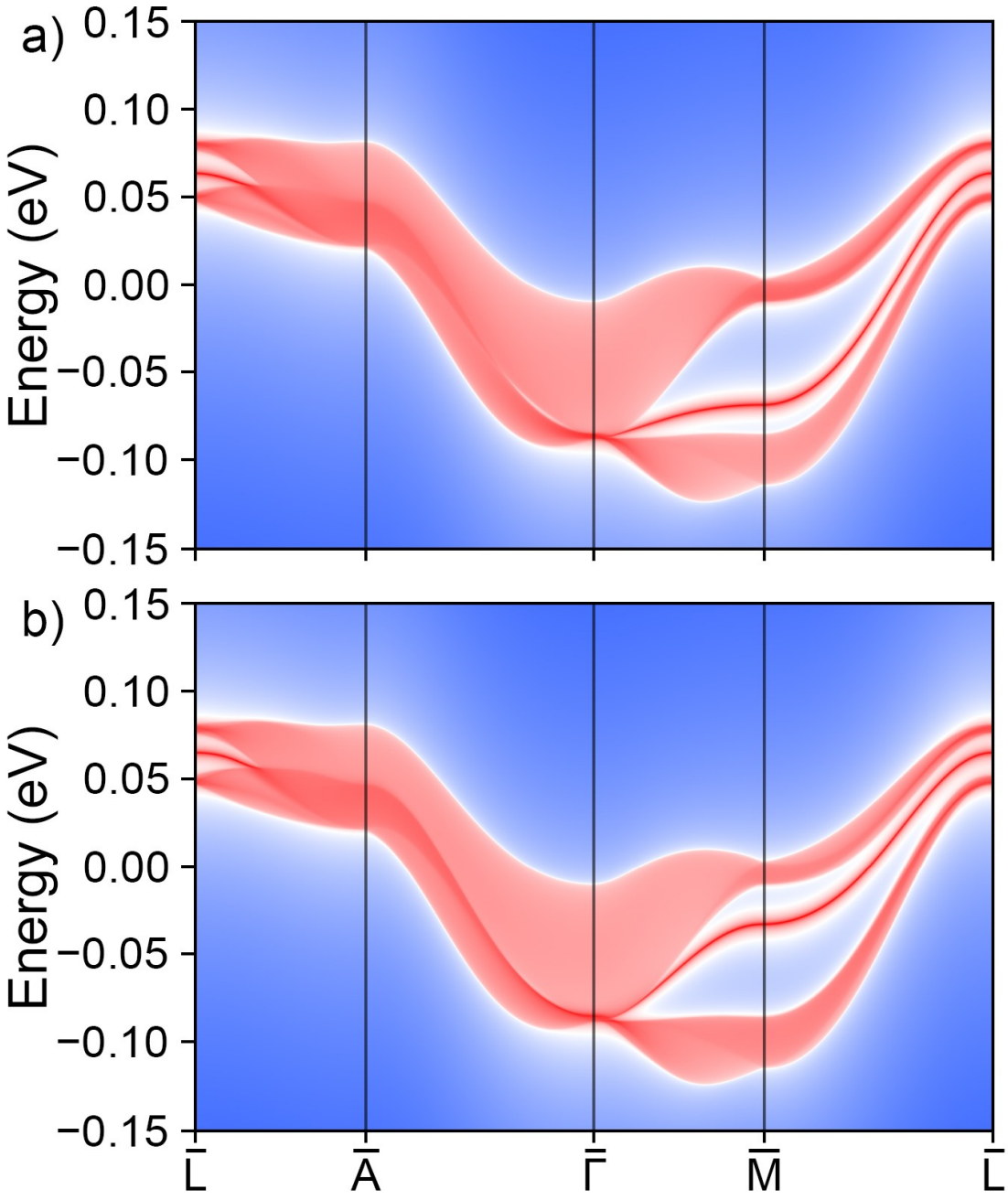

Figure S13. The projected surface states of the Ag-doped lead apatite $Pb_9Ag(PO_4)_6O$ in (110) plane for top a) and bottom b) terminations. Clear surface arc states connecting the Weyl points between at $\bar{\Gamma}$ and $\bar{A}$ positions can be easily distinguished from the bulk band states for both termination conditions.

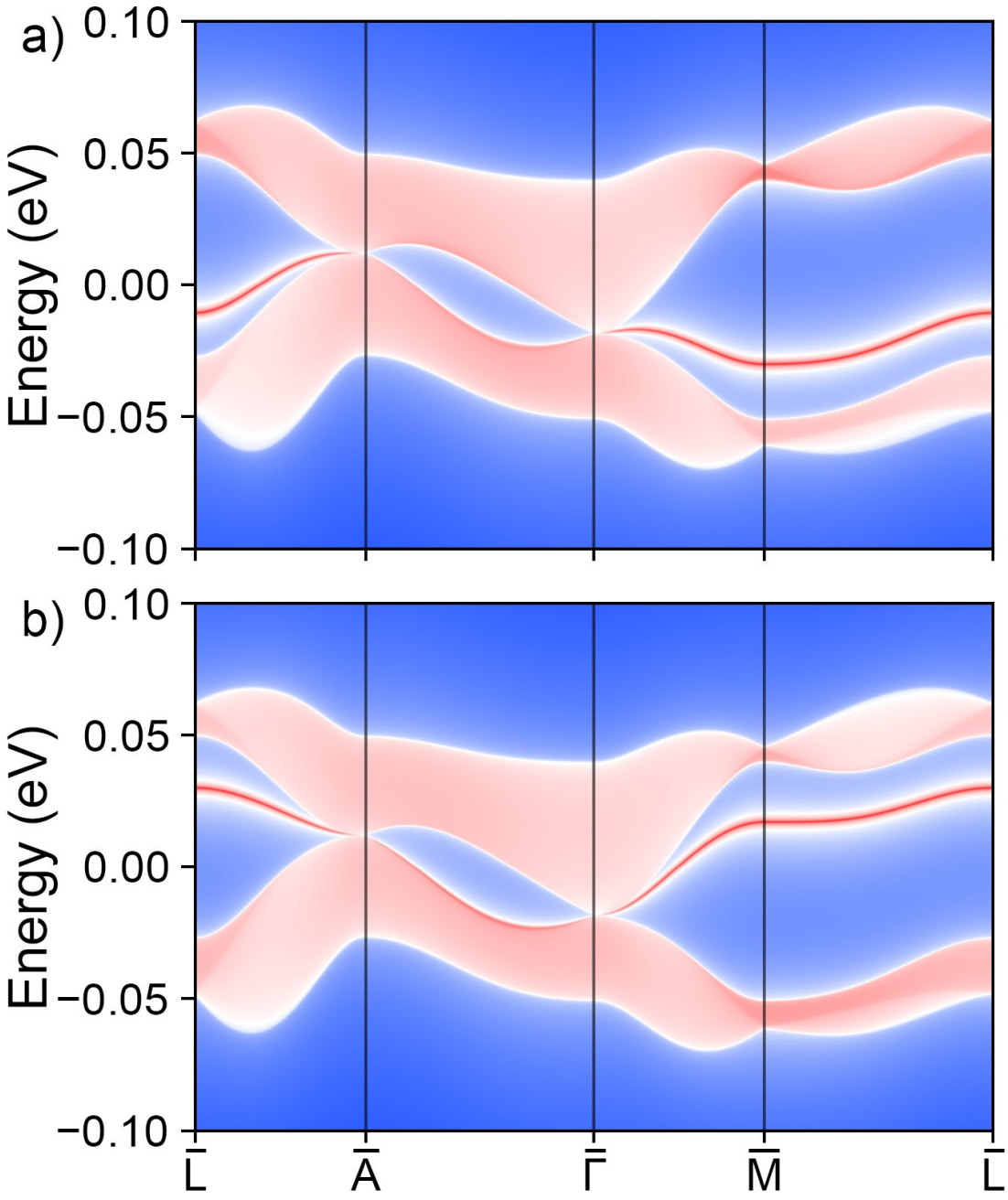

Figure S14. The projected surface states of the Au-doped lead apatite $Pb_9Au(PO_4)_6O$ in (110) plane for top a) and bottom b) terminations. Clear surface arc states connecting the Weyl points between at $\bar{\Gamma}$ and $\bar{A}$ positions can be easily distinguished from the bulk band states for both termination conditions.

Table S1. The various independent elastic constants (C_{ij}), Young's modulus (E), shear modulus (G), linear compressibility (β) and Poisson's ratio (ν) of the $Pb_9Cu(PO_4)_6O$.

C_{11}	C_{12}	C_{13}	C_{14}	C_{15}	C_{33}	C_{44}	E	G	β	ν
(GPa)									(TPa^{-1})	
235.54	79.28	69.84	-6.29	6.65	234.29	65.49	184.57	73.37	2.65	0.2578